Yi Yang, Ching-Tai Ng, Andrei Kotousov, Hoon Sohn, Hyung Jin Lim
Second harmonic generation at fatigue cracks by low-frequency Lamb waves: experimental and numerical studies
Mechanical Systems and Signal Processing, 2018; 99:760-773

Second harmonic generation at fatigue cracks by low-frequency Lamb waves: experimental and numerical studies

Yi Yang[a], Ching-Tai Ng[a,*], Andrei Kotousov[b], Hoon Sohn[c], Hyung Jin Lim[c]

[a] *School of Civil, Environmental and Mining Engineering, The University of Adelaide, Adelaide, SA 5005, Australia*

[b] *School of Mechanical Engineering, The University of Adelaide, Adelaide, SA 5005, Australia*

[c] *Department of Civil and Environmental Engineering, KAIST, Daejeon, 305-701, South Korea*

Abstract

This paper presents experimental and theoretical analyses of the second harmonic generation due to non-linear interaction of Lamb waves with a fatigue crack. Three-dimensional (3D) finite element (FE) simulations and experimental studies are carried out to provide physical insight into the mechanism of second harmonic generation. The results demonstrate that the 3D FE simulations can provide a reasonable prediction on the second harmonic generated due to the contact nonlinearity at the fatigue crack. The effect of the wave modes on the second harmonic generation is also investigated in detail. It is found that the magnitude of the second harmonic induced by the interaction of the fundamental symmetric mode (S_0) of Lamb wave with the fatigue crack is much higher than that by the fundamental anti-symmetric mode (A_0) of Lamb wave. In addition, a series of parametric studies using 3D FE simulations are conducted to investigate the effect of the fatigue crack length to incident wave wavelength ratio, and the

* Corresponding author: alex.ng@adelaide.edu.au

influence of the excitation frequency on the second harmonic generation. The outcomes show that the magnitude and directivity pattern of the generated second harmonic depend on the fatigue crack length to incident wave wavelength ratio as well as the ratio of S_0 to A_0 incident Lamb wave amplitude. In summary, the findings of this study can further advance the use of second harmonic generation in damage detection.

Keywords: nonlinear Lamb wave, second harmonic, fatigue crack, contact nonlinearity, finite element method, experimental study

1 Introduction

1.1 Lamb waves

Over the lifespan, engineering structures accumulate mechanical damage due to fatigue, temperature variations, effects of aggressive environment and aging. Without proper inspection and maintenance strategies to ensure the safety and integrity of the structures, the accumulation of the damage can lead to catastrophic consequences. Therefore, the development and deployment of non-destructive evaluation (NDE) and structural health monitoring (SHM) are critical to ensure the structural safety, minimize the maintenance costs, and extend the service life of the structures.

Among various NDE and SHM techniques, Lamb wave has attracted significant attention due to its outstanding properties, such as ability to propagate a long distance, able to provide rapid inspection, high sensitivity to many types of mechanical damages, and detection of damages at inaccessible at locations [1]-[4]. In the last two decades, different Lamb wave based techniques [5]-[9] have been developed for damage detection. The majority of the developments

focused on linear Lamb wave that determines the presence of damage based on the change of wave speed, reflection and transmission, or mode conversion [10] of the linear wave signals, i.e. the scattered wave at the same frequency as the incident wave [11]-[13]. The linear features of Lamb wave are sensitive to damages with sizes comparable to the wavelength of the incident wave, e.g. corrosion spot [14][15] or crack [17][18]. However, they are not effective in detecting early stage of mechanical damage, e.g. micro-damage and small fatigue crack. In addition, most of the damage detection techniques based on the linear Lamb wave require baseline data [19] to extract the scattered wave signal from the damage. But the change of environmental conditions, e.g. temperature variation [20]-[22], stress level [23] could make the baseline subtraction fail in extracting the scattered waves signal from the damages. Therefore, there is a need to overcome the aforementioned deficiencies of the linear wave signals to achieve effective and practical damage detection.

1.2 Nonlinear Lamb waves

Nonlinear ultrasonic techniques detect the incipient damage based on nonlinear phenomena, such as higher harmonic generation [24], sub-harmonic generation [25], mixed frequency response [26],[27] and nonlinear resonance [28]. A number of studies have demonstrated that the nonlinear characteristics and phenomena are more sensitive to the presence of contact-type damage, such as fatigue crack and delamination, and have less influence by environmental change than the linear features.

Early developments of the nonlinear ultrasonic techniques focused on the nonlinearity of elastic bulk waves [29]-[31]. Recently, several studies have focused on the nonlinearity of Lamb waves [32]. Compared to the nonlinear ultrasonic techniques based on the bulk waves, nonlinear

Lamb waves could provide long-range inspection for thin-wall structures. A number of studies have demonstrated that the generation of second- or third-order harmonics could be used to determine the presence and severity of incipient damage in structures [33]. The generation of higher harmonics involves various non-linear phenomena. However, recent studies have primarily focused on the investigations of the higher harmonic generation due to nonlinear elasticity [24] and contact nonlinearity [35][36].

The early damage accumulation usually leads to the deviation of the stress-strain behavior from the linear Hook's law. The higher harmonics are generated due to this nonlinearity in the elastic behavior of the material, and this provides a way for the measurement and quantification of the micro-damage. The material nonlinearity normally leads to distortion of propagating waveforms, and hence, it generates the higher harmonic. A number of studies focused on the material nonlinearity were performed by several researchers [24], [34], [35]-[39].

Lamb waves are dispersive and have multi-mode nature, which make accurate experimental realization of nonlinear Lamb wave become difficult. As illustrated in the aforementioned studies, the phase and group velocity matching are essential conditions to generate cumulative behavior of the second harmonic, i.e., the magnitude of second harmonic increases with wave propagation distance [24]. These conditions ensure that the second harmonic Lamb wave can propagate a reasonably long distance and can be detected. Pruell *et al.* [34] found that the plasticity-induced damage can cause the second harmonic generation. Li *et al.* [37] employed the second harmonic Lamb waves to assess thermal fatigue damage in composite laminates. Zhou *et al*. [38] carried out an experiment study to demonstrate that the higher harmonic Lamb wave can be used to evaluate the fatigue crack. They found that the nonlinearity

contributed by the material itself, i.e. the nonlinear elasticity effect, is insignificant compared with that induced by the fatigue damage.

When Lamb wave interacts with contact-type of damage, e.g. fatigue crack [35] and delamination [40],[41], higher harmonics can be generated due to the contact nonlinearity. This happens due to the nonlinear interaction of the crack surfaces caused by the incident Lamb wave. When the incident wave passes through the crack, the compressive pressure of the incident wave closes the crack and the tensile pressure opens the crack. As a result, the compressive part of the incident wave penetrates the crack, while the tensile part cannot. This phenomenon is schematically illustrated in Fig. 1. This clapping behavior at the crack surfaces causes the nonlinearity, and hence, generating the higher harmonics due to the effect of localized nonlinearity [33].

[Fig. 1: Concept of contact nonlinearity at a fatigue crack]

A number of studies have investigated the generation of higher harmonics by low-frequency incident guided wave, i.e. below 500 kHz. Nucera and Lanza di Scalea [42] investigated the nonlinear guided wave in multi-wire strands. They demonstrated that the higher harmonics generated by the inter-wire contact at different axial load levels. Two- (2D) and three-dimensional (3D) finite element (FE) simulations considered the contact nonlinearity arising from the inter-wire stresses between individual wires comprising the strand were carried out to study the higher harmonic generation. Experimental study was conducted to verify this phenomenon. Shen and Giurgiutiu [35] proposed a 2D FE model to study the nonlinear guided waves generated by low-frequency incident wave interaction with a breathing crack. They

considered the effect of contact nonlinearity in their model and investigated the generation of higher harmonics by the fundamental symmetric (S_0) and anti-symmetric (A_0) mode of Lamb wave. They also demonstrated that the FE model is capable to describe the nonlinear wave propagation phenomenon. Soleimanpour and Ng [40] investigated the higher harmonic generated by A_0 mode Lamb wave interaction with a delamination in laminated composite beams. A 3D FE model with the contact nonlinearity at the delamination was used to study the generation of the higher harmonics. The FE model was experimentally verified and then applied to investigate the higher harmonic generation. Yelve *et al*. [41] investigated the higher harmonics generation by the interaction of S_0 Lamb wave with a delamination. A 2D FE model with contact effect at the surfaces of the delamination was used to investigate the higher harmonic generation. In addition, experimental studies were also carried out to further validate the results. They demonstrated that the contact nonlinearity could generate higher harmonics.

The aforementioned studies with the low-frequency incident Lamb wave did not require the phase and group velocity matching for generating the cumulative higher harmonics. Therefore, the main contribution to the higher harmonic generation was mainly due to the contact nonlinearity at the contact surfaces of the damage. In general, the use of the low-frequency incident Lamb wave to detect the damage based on the higher harmonic generation due to contact nonlinearity is easier to be experimentally achieved than that of due to material nonlinearity. This is because the contact nonlinearity does not require highly accurate experimental procedure and sophisticated equipment to satisfy the phase and group velocity matching condition. In addition, Lamb wave at low excitation frequency range only has S_0 and A_0 mode, therefore, the excitation will not induce higher-order modes of Lamb wave for both incident and higher harmonic Lamb

wave. Hence, it does not require advanced signal processing and experimental techniques to extract the higher harmonic information from the measured data.

Currently there are limited studies focused on the higher harmonic generation of Lamb wave at the fatigue crack due to contact nonlinearity, especially for study using both 3D FE simulations and experimentally measured data. Moreover, the majority of the previous studies focused on the situation when fatigue crack is oriented perpendicular to the incident wave propagation direction, i.e. only forward and backward directions of the higher harmonic Lamb wave were studied. In practical applications where transducer arrays are used for damage detection, the fatigue crack can be oriented at different angles with respect to the incident wave direction. Different magnitudes of higher harmonic Lamb waves could be generated at different scattering angles. Therefore, it is important to gain a physical insight into the higher harmonics generated by contact nonlinearity at the fatigue crack. The insight can further advance the use of the higher harmonic Lamb waves for damage detection, specifically for small-scale and micro-damage.

In this study, comprehensive 3D FE simulations and experimental studies are carried out to investigate the second harmonic generation at the fatigue crack due to the contact nonlinearity using S_0 and A_0 Lamb wave. The magnitude of the higher harmonics generated by S_0 and A_0 Lamb wave is investigated in detail. In addition, this study investigates the directivity pattern of the higher harmonic generation. This provides further understanding of the higher harmonic generation phenomenon.

This study also demonstrates the feasibility of using the 3D FE simulation to predict the higher harmonics generation due to Lamb wave interaction with the fatigue crack. The FE simulation provide many benefits, such as substantial reduction of time and cost in the

investigations. Noticeably, there are other numerical simulation techniques, such as boundary element method (BEM), finite difference (FD) method and spectral finite element method (SFE) method, for solving guided wave propagation problems [43]. Apart from FE method, SFE method has also attracted attention in the last decade [44]-[46]. This method is more computational efficient compared with FE method, especially for simulating high frequency wave propagation where the required element size for ensuring the accuracy of the FE simulation becomes very small. However, FE simulation has been commonly used to simulate guided wave propagation problems [16], [35], [38] due to its ability in modelling complex geometries [43] and the availability of well-established commercial software programs. Therefore, this study employs the FE simulation to study the second harmonic generation.

The paper is organized as follows. Section 2 describes the details of the 3D explicit FE simulations, which include the actuator and sensor model, and modeling of the fatigue crack. Section 3 presents the experimental validation, which describes the details of the fatigue crack generation through cyclic tests, experimental setup for actuating and sensing the Lamb wave, and mode-tuning results for generating a specific mode of Lamb wave. Section 4 discusses the results obtained from the numerical simulations and experiments. Section 5 presents a parameter study considering different incident wave wavelength to crack length ratios. The paper also presents a comprehensive study of the magnitude and scattering directivity pattern of the second harmonic generation. Finally, conclusions are drawn in Section 6.

2 Three-dimensional Explicit Finite Element Simulation

The Lamb wave propagation and interaction with the fatigue crack in an aluminum plate was modeled using a 3D explicit FE method. The dimensions of the aluminum plate are

300mm×200mm×3mm. Eight piezoceramic discs with 10mm diameter and 0.5mm thickness were modeled on the surface of the aluminum plate to excite and measure the Lamb wave signals. The materials of the aluminum plate and piezoceramic discs are 5005-H34 aluminum and Pz27, which are the same as the specimen used in experiment in Section 3. The Young's modulus, Poisson's ratio and density of 5005-H34 aluminum are 69.5GPa, 0.33 and 2700kg/m^3, respectively. The material properties of the piezoceramic discs are shown in Table 1. The eight piezoceramic discs, which are labeled as PZT1–PZT8, form a 50mm diameter circular transducer network as shown in Fig. 2. Based on the polar coordinate shown in the Fig. 2, they are located at r = 50mm and θ = 0° (PZT1), 45° (PZT2), 90° (PZT3), 135° (PZT4), 180° (PZT5), 225° (PZT6), 270° (PZT7) and 315° (PZT8), respectively. The same configuration of the transducer network was also used in the experimental studies and it will be described in the next section. In this study, PZT5 was used to actuate Lamb waves while the rest of the piezoceramic discs were used for sensing.

[Table 1: Material properties of the model piezoceramic discs]

[Figure 2: Schematic diagram of the FE simulations and experiments]

Commercial FE software, ABAQUS/CAE, was used to construct the 3D FE model. Eight-noded 3D fully integrated linear brick elements, C3D8I, in which each node has three translational degrees-of-freedom (DoFs), were used to model the aluminum plate and the piezoceramic discs. The in-plane dimensions and the thickness of the elements are around 0.4mm×0.4mm and 0.375mm, respectively, so that there are at least 20 elements per wavelength

for the incident and generated second harmonic Lamb wave. In the thickness direction of the aluminum plate, there are eight layers of the brick elements. The aspect ratio of the brick elements is 1.07. The simulation was solved using the explicit FE code, ABAQUS/Explicit, which employs the explicit central different integration scheme to calculate the response of the wave propagation. The excitation signal is a sinusoidal tone burst pulse modulated by a Hanning window, which is applied to the actuator model described in next sub-section to excite the Lamb wave in the aluminum plate.

2.1 Actuator and sensor model

In this study, the piezoceramic discs used for excitation and measurement were modeled using 3D brick elements in the FE simulations with the consideration of the direct and converse piezoelectric effects. The bonding between the piezoceramic discs and the aluminum plate is assumed to be perfect, and hence, the strain is continuous at interface between the piezoceramic disc and the aluminum plate. The radial displacement at the circumference of the actuator has a linear relationship with the input voltage [47][48] as

$$d_r = R\frac{d_{31}}{h_{PZT}}\left[\frac{\tilde{E}(1-\nu_{PZT})}{E_{PZT}} + 1\right]V_{in} \tag{1}$$

where V_{in} is the applied voltage. d_{31}, R, E_{PZT}, ν_{PZT} and h_{PZT} are charge constant, radius, Young's modulus, Poisson's ratio and thickness of the piezoceramic discs, respectively. $\tilde{E}$ is a constant related to the material properties and thickness of the plate and piezoceramic disc, and it is given in [48]. The excitation signal in the form of voltage is converted to displacement based on the material properties of the piezoceramic discs using Eq. (1) and is then applied to the FE nodes of the piezoceramic disc to generate the Lamb wave.

For the sensor model, the output voltage is related to the radial and tangential strains [47][48] of piezoceramic discs as

$$V_{out} = \frac{d_{31} E_{PZT} h_{PZT}}{4\pi K_3 p_0 R^2 (1 - \nu_{PZT})} \iint (\varepsilon_r + \varepsilon_\theta) r_{PZT} dr_{PZT} d\theta_{PZT} \tag{2}$$

where r_{PZT} and θ_{PZT} are the radial and tangential direction, respectively, of the polar coordinate located at the center of each piezoceramic disc. K_3 is the dielectric constant of the piezoceramic discs, p_0 is the dielectric permeability. ε_r and ε_θ are radial and tangential strain component, respectively. Integrating Eq. (2) with respect to r_{PZT} and θ_{PZT}, we can obtain

$$V_{out} = \frac{d_{31} E_{PZT} h_{PZT}}{4 K_3 p_0 (1 - \nu_{PZT})} (\varepsilon_r + \varepsilon_\theta) \tag{3}$$

Hence, the measured voltage by the sensor could be obtained from the strain of the brick elements that used to model the piezoceramic discs in the FE simulations.

2.2 Modelling of fatigue crack

The fatigue crack was modeled by embedding a seam crack at the fatigue crack position in the aluminum plate model. Fig. 3 shows a schematic diagram of the fatigue crack model. The fatigue crack was modeled by duplicating and overlapping the nodes along the seam crack, and hence, it is originally closed but it could be opened when Lamb waves interacting with the fatigue crack. Hard normal contact and friction tangential contact are applied to the interfaces of the seam crack to prevent nodes penetration, and hence, simulating the breathing behavior when the Lamb wave interacts with the fatigue crack. A typical friction coefficient of aluminum [49] is used and the value is slightly increased to take into account the roughness of the actual fatigue crack surfaces. In this study, a friction coefficient of 1.5 was used to simulate the relative sliding of the fatigue crack surfaces. For the experiment validation in the next section, the fatigue crack was generated

and controlled using a circular through hole with starter notches in the fatigue loading process. For validating the FE model with the experimental measurements, the circular through hole and the starter notches are also modeled by removing the elements in the FE model.

[Figure 3: FE model of the fatigue crack for simulating the a) experimental condition, and b) numerical parametric study]

3 Experiment

3.1 Fatigue test

Two 300mm×200mm×3mm 5005-H34 aluminum plates having the same material properties as the plate model in the FE simulations were used in the experiment. A 5mm diameter circular through hole was machined at the center of one of the aluminum plates and two 2mm long starter notches were cut using a 1mm thick saw blade. One of the plates was subjected to a sinusoidal tensile load in an INSTRON 1432 testing machine. The cyclic tension load was applied with a minimum of 5kN and a maximum of 40kN with a frequency of 10Hz. The plate was inspected every 5,000 cycles of loading and it took approximately 60,000 cycles to initiate the fatigue crack at the end of the starter notch. The cyclic loading process was stopped when the fatigue cracks propagate to approximately 10mm long as shown in Fig. 4. The other aluminum plate was used as the control specimen, and hence, it is an intact aluminum plate. It is used to quantify the second harmonic induced from non-damage related effects, such as material nonlinearity, the interaction between transducers and host plate, and instrumentation chain, etc.

[Figure 4: Fatigue testing using INSTRON and the fatigue crack generated at the end of the starter notches]

3.2 Experimental setup for actuating and sensing Lamb wave

Eight 10mm diameter and 0.5mm thick piezoceramic discs (Ferroperm Pz27) were bonded to the surface of the aluminum plates using conductive epoxy for exciting and sensing the Lamb wave. The piezoceramic discs were installed after the completion of the fatigue testing to avoid the possible degradation of the adhesive layers between the surface of the piezoceramic discs and the plate during the fatigue testing. The material properties and positions of the piezoceramic discs were the same as those in the FE simulations. A computer controlled signal generator NI PIX-5412 was used to generate a narrow-band sinusoidal tone burst pulse modulated by a Hanning window and it was applied to the PZT5 (r = 50 mm and θ = 180°) as shown in Fig. 2 to generate the Lamb wave. The peak-to-peak voltage of the output signal is 10V. It was amplified by a factor of 5 using an amplifier (KROHN-HITE 7500) before it was sent to the PZT5. The rest of the piezoceramic discs (PZT1-PZT4 and PZT6-PZT8) were used to measure the Lamb wave. The signals measured by the piezoceramic discs were digitized by a data acquisition system (NI PXIe-5105) and then fed into the computer. The sampling rate was 6 MHz and the quality of the measurements was improved by averaging the signals in the time domain with 64 acquisitions.

3.3 Mode-tuning of Lamb wave

In this study, the second harmonic generation by the interaction of S_0 and A_0 Lamb waves at fatigue cracks were investigated individually. A mode-tuning experiment [50] was first carried out to determine the optimal excitation frequencies that could maximize the amplitudes of the S_0

and A_0 mode responses, respectively. A pair of piezoceramic discs with 10mm diameter and 0.5mm thickness were attached to the surface of a 1000mm×1000mm×3mm aluminum plate with the same material properties as those used in the fatigue testing. The 4-cycle narrow-band sinusoidal tone burst pulse modulated by a Hanning window swept from 10kHz to 400kHz in steps of 20kHz was applied to one of the piezoceramic discs to generate the Lamb wave and the rest of the piezoceramic discs were used for measurements. At each excitation frequency, the amplitudes of the S_0 and A_0 Lamb wave were recorded. Fig. 5 shows the mode-tuning results. The A_0 Lamb wave is dominant at low excitation frequencies. The amplitude of the S_0 Lamb wave increases with the excitation frequency and has similar magnitude as the A_0 Lamb wave at 160kHz. The S_0 Lamb wave then becomes dominant at higher excitation frequencies. As shown in Fig. 5, the ratios of A_0 to S_0 and S_0 to A_0 Lamb wave amplitudes are maximized at 30kHz and 240kHz, respectively. Therefore, the excitation frequency of 30kHz and 240kHz were chosen to excite the dominated A_0 and S_0 Lamb wave in the rest of the study, respectively.

[Figure 5: Lamb wave mode-turning curve for 3mm thickness 5005-H34 aluminum plate excited by a 10mm diameter and 5mm thick piezoceramic disc]

3.4 A_0 and S_0 Lamb wave

In this section the FE simulated and experimentally measured A_0 and S_0 Lamb wave are compared. Based on the mode-tuning results in Section 3.3, the 30 kHz and 240kHz narrow-band sinusoidal tone burst pulse modulated by a Hanning window were applied separately to the PZT5 of the transducer network to generate Lamb wave in the intact aluminum plate. Fig. 6 shows a comparison between the numerical simulated and experimentally measured 30kHz A_0 and

240kHz S_0 Lamb wave at PZT2 and PZT4. Both of the numerical simulated and experimentally measured Lamb wave signals are normalized with respect to their maximum values. The results show that there is good agreement between the numerically simulated and experimentally measured A_0 and S_0 Lamb wave.

[Figure 6: Numerical simulated and experimental measured Lamb wave signal, a): 30 kHz wave at PZT2, b): 30kHz wave at PZT4, c): 240kHz wave at PZT2, and d): 240kHz wave at PZT4]

4 Results and Discussions

Experimental measurements of the second harmonic generation were carried out using the two aluminum plates described in Section 3.1, i.e. the intact plate and the plate with 10mm long fatigue cracks generated at the end of the starter notches of the circular hole. The number of cycles for excitation signals was increased to eight cycles to reduce the excitation frequency bandwidth in frequency domain. This ensures the generated second harmonic would not overlap with the excitation frequency components in the frequency domain. The 30kHz and 240kHz excitation signals were applied to the PZT5 to generate the A_0 and S_0 dominated Lamb wave, respectively. The rest of the piezoceramic discs in the transducer network were used for measurements.

The measured signals in both experiments and FE simulations have the same total duration, i.e. 1.6ms, which covers the incident and reflected signals from boundaries. The measured signals were then transformed to the frequency domain using Fast Fourier Transform (FFT). The spectra of the signals measured by PZT6 for the incident A_0 and S_0 Lamb wave in the intact and the plate with the fatigues cracks are shown in Figs. 7a and 7b, respectively. As shown in Fig. 7,

the spectra of A_0 and S_0 incident Lamb waves have maximum values around their excitation frequencies, i.e. 30kHz and 240kHz, respectively. As described in Section 1, the second harmonic would occur at the double of the excitation frequency, i.e. 60kHz and 480kHz for the A_0 and S_0 incident Lamb wave used in this study, respectively. However, Fig. 7a shows that only a small magnitude of second harmonic is generated by the incident A_0 Lamb wave interacting with the fatigue crack. For the results of the S_0 incident Lamb wave as shown in Fig. 7b, the magnitude of the second harmonic at 480kHz can be clearly observed. However, the result of the intact plate still has a very small magnitude of the non-damaged related second harmonic. These non-damaged related nonlinearities were possibly caused by intrinsic material nonlinearity, connections between plate and transducers, instrumentation or background noise. Since the magnitude of the non-damaged related nonlinearities is much smaller than the second harmonic generated by the interaction of the Lamb wave with the fatigue crack, it was ignored in this study.

For the third harmonic of the Lamb waves, i.e. at 90kHz for A_0 Lamb wave and 720kHz for S_0 Lamb wave, both undamaged plate and the plate with the fatigue crack have similar amplitudes. In the literature, a spectral damage index [51] was proposed to take into account the generation of third and fourth harmonic at a breathing crack. In their study, the energy of the fundamental harmonic is transferred to higher harmonics due to intensive contact nonlinearity at the breathing crack. However, for the present study, the amplitude of the third harmonic is less than 1% of the amplitude of the second harmonic, the generated third harmonic can be neglected in this study.

[Figure 7: Spectra of the signals measured from PZT6 of the intact plate and the plate with the fatigue crack for the incident a) A_0 (30kHz) and b) S_0 Lamb wave (240kHz)]

There are four possible sources of nonlinearity, (i) contact nonlinearity at the crack, (ii) nonlinear elasticity of material, (iii) inherent nonlinearity of electrical equipment, and (iv) background noise. In general, the contact nonlinearity at the crack is usually much larger than the other three possible sources of nonlinearity [52]. Therefore, the higher harmonic induced by the crack is usually dominant in the measured signal, and hence, it is assumed that the second harmonic is mainly contributed by the contact nonlinearity. In this study a relative nonlinear parameter β_C' is defined to quantify the generation of the second harmonic due to the contact nonlinearity at the fatigue crack. The relative nonlinearity parameter β_C' is defined as [52]

$$\beta_C' = \frac{A_2}{A_1^2} \tag{4}$$

where A_1 and A_2 are the magnitude of fundamental component and second harmonic component estimated from the Fourier transform of the measured signal at the piezoceramic disc. In both FE simulations and experimental studies, β_C' of the data measured by each piezoceramic disc is normalized by the mean of β_C' of all piezoceramic discs.

4.1 Effect of incident wave modes

Fig. 8 shows the calculated values of the nonlinear parameter obtained by using 240kHz (S_0 dominated), 160kHz (S_0 and A_0 mixed) and 30kHz (A_0 dominated) incident waves. The relative nonlinear parameter of the measured signals from the sensor on the damaged plate (β_C') is normalized to the corresponding value obtained from the intact plate (β_{C0}'). For the S_0 Lamb

wave (i.e. at 240kHz), the value of the normalized relative nonlinearity parameter is much larger than 1 at all transducers, which indicates the presence of fatigue cracks in the plate.

At 160kHz as shown in the mode-tuning curve (Fig. 5), the incident wave contains similar magnitudes of A_0 and S_0 incident Lamb wave. According to Fig. 8, the values of normalized relative nonlinear parameter are all larger than 1. Although the value is much smaller than the case when S_0 dominated incident Lamb wave is used, it can still be used to indicate the fatigue crack.

For the results at 30kHz, i.e. A_0 dominated incident wave, the value of the normalized relative nonlinear parameter is less than 1 at most of the sensors. This demonstrates that there is not much second harmonic generated due to the contact nonlinearity at the fatigue crack when A_0 dominated incident Lamb wave is used. Overall, the results indicate that the S_0 dominated incident Lamb wave could generate relative large magnitude of second harmonic compared to A_0 dominated, and S_0 and A_0 mixed incident Lamb wave.

[Figure 8: Normalized relative nonlinear parameter obtained at all transducers on damaged plate using 240kHz (S_0) and 160kHz and 30kHz (A_0) Lamb waves]

4.2 Comparison of results between finite element simulations and experiments

As discussed in the previous section, using the A_0 dominated incident Lamb wave (30kHz) does not generate much second harmonic as compared to the results of using either S_0 (240kHz) dominated or S_0 and A_0 mixed (160kHz) incident Lamb wave. Therefore, the comparison between the experimental and FE results only focuses on the S_0 dominated and S_0 and A_0 mixed

incident Lamb wave at 240kHz and 160kHz, respectively. There are some discrepancies between the experimentally and numerically obtained normalized relative nonlinear parameter due to the facts that:

1. The fatigue crack in experiment could be initially open or partially closed, and hence, a certain amount of wave energy is used to close and re-open the crack. While in FEM, the crack surfaces are initially closed.
2. The crack is modeled as two straight lines in the FE model with an assumed value of friction factor between crack contact surfaces. While the actual shape of fatigue crack is not perfectly straight, and the friction factor and interaction behavior might vary along the fatigue crack in the experiment.
3. The nonlinearities as discussed at the beginning of Section 4, were not fully modelled. Though these nonlinearities are small compared with the contact nonlinearity, they may also contribute to the discrepancy between the experimental and numerical results.

It is difficult to perfectly predict the actual values of β_C' considering the aforementioned factors. Instead, the directivity patterns of the β_C' at different sensors are studied, which provide useful information about the scattering feature of the nonlinear Lamb wave at the fatigue crack. In the rest of this section, the β_C' value measured at each piezoceramic disc is normalized to the averaged β_C' values of all piezoceramic discs for the FE and experimental results. As shown in Fig. 9, there is good agreement between FE simulated and experimentally measured second harmonic directivity patterns when S_0 (240kHz) and S_0 and A_0 mixed (160kHz) incident Lamb wave are used. It can be seen that the normalized relative nonlinear parameters of PZT2, PZT3 and PZT4 have very similar magnitudes to the PZT8, PZT7, PZT6, respectively, as they are

located symmetrically about the incident wave propagation direction (perpendicular to the fatigue crack) in the FE simulations. Fig. 9 shows that the experimentally obtained values of the relative nonlinear parameters for the aforementioned piezoceramic transducers are not distributed as symmetric as the FE results. This is because the generated fatigue cracks at both ends of the starter notches are perfectly the same in the FE simulation but they are different in the experiment. Fig. 9 also shows that there is a small level of asymmetric distribution of the relative nonlinear parameter in the FE results. It is mainly due to the fact that the size and shape of the elements in this region of the FE model are similar but they are not perfectly the same.

While loading the specimen to initiate the fatigue crack in cyclic test, the specimen undergoes material degradation, e.g., loss of stiffness and dislocation of grains [34],[53]. This can induce the material nonlinearity and cause a slight difference between the FE calculated and the experimentally measured directivity patterns as the FE simulations do not take into account the material nonlinearity. As this study does not follow the phase and group velocity requirement, the higher harmonics generated by the material nonlinearity are not accumulated, i.e. decay with the wave propagation distance. Hence, the higher harmonics generated by the material nonlinearity is minimized in this study. Overall, the comparison between the FE simulation and experimental results show that the FE simulation is able to provide a reasonable prediction of the higher harmonic generation at the fatigue crack by the low frequency Lamb wave.

[Figure 9: FE simulated and experimentally measured normalized relative nonlinear parameter at a) 240kHz (S_0 Lamb wave); and b) 160kHz (S_0 and A_0 mixed Lamb wave)]

5 Parametric study

5.1 Effect of varying crack length

In this section, the experimentally verified FE model is used to study the second harmonic generation measured at different sensors for different crack lengths using 240kHz S_0 incident Lamb wave. In addition to the eight transducers, i.e. PZT1-PZT8, as shown in Fig. 2, an additional transducer is added at r = 80mm and θ = 180° to act as the actuator. As shown in Fig. 3b, only the fatigue crack was modeled in the FE simulation, i.e. without the through hole and the starter notches. The simulation duration is 5.2μs, which only covers the incident Lamb wave propagates from the actuator to the fatigue crack, and then, the generated second harmonic Lamb wave propagates from the fatigue crack to the sensors. In this section the relative nonlinear parameter β_C' is normalized to the value obtained from the corresponding sensors at intact state (β_{C0}').

As shown in Fig. 10, only the normalized relative nonlinear parameter obtained at PZT1 (0°) grows linearly with fatigue crack length to incident wave wavelength ratio. For other sensors, the increase of the magnitude of the normalized relative nonlinear parameters is slower than the results of PZT1, especially for PZT3 (90°) and PZT7 (270°). At PZT2 (45°), PZT4 (135°), PZT6 (225°) and PZT8 (315°), the normalized relative nonlinear parameter decreases when the fatigue crack length to incident wave wavelength ratio increases beyond 0.3. The results demonstrate the importance of designing the transducer network, as the damage information might be misinterpreted or overlooked for sensors at some particular locations.

[Figure 10: Normalized relative nonlinear parameter as a function of fatigue crack length to incident wave wavelength ratio]

The directivity patterns of the normalized relative nonlinear parameters for cracks with length equals to 4mm, 8mm, 12mm and 16mm are shown in Fig. 11. The directivity patterns indicate that the magnitude of the normalized relative nonlinear parameter mainly concentrates in forward and backward scattering directions of the second harmonic Lamb wave. Meanwhile, as the crack length increases, the magnitude of the second harmonic Lamb wave is dominated in the direction at θ = 0° and 180°.

[Figure 11: Directivity pattern of normalized relative nonlinear parameters for a) 4mm; b) 8mm; c) 12mm; and d) 16mm long fatigue crack]

5.2 Effect of varying excitation frequency

The other parametric study was carried out by varying excitation frequency and the results are shown in Fig. 12. The frequency is varied from 200kHz to 400kHz, in which the amplitude of S_0 incident Lamb wave is higher than that of the A_0 incident Lamb wave based on the mode-tuning curve as shown in Fig.5. The crack length is fixed at 8mm. Without loss of generality, the results are presented in terms of fatigue crack length to incident wave wavelength ratio. It is found that the variation of β_C' has a similar trend to the variation of the ratio of S_0 to A_0 incident Lamb wave amplitude. For most of the transducers, except transducers at 45^o (PZT2) and 315^o (PZT8), the value of β_C' reaches the maximum when fatigue crack length to incident wave wavelength ratio equals to 0.371, which is corresponding to the excitation frequency of 250 kHz. At this frequency, the ratio of S_0 to A_0 incident Lamb wave amplitude becomes about maximum as shown in Fig. 5. For the transducers at 45^o and 315^o, β_C' reach its maximum value when the fatigue crack length to

incident wave wavelength ratio equals to 0.447 (300kHz), and this frequency is close to the frequency, 280kHz, at which the S_0 incident Lamb wave becomes maximum at this frequency as shown in Fig. 5. The results again illustrate that larger magnitude of the S_0 incident wave tends to generate larger magnitude of second harmonic at the fatigue crack. The directivity pattern of β_C' is also investigated and they are shown in Fig.13. In general, the directivity patterns show that the amplitude of β_C' in the forward scattering direction has relative larger magnitude compared to other directions.

[Figure 12: Variation of normalized relative nonlinear parameter against the crack length to incident wave wavelength ratio]

[Figure 13: Directivity patterns of normalized relative nonlinear parameters at different crack length to incident wave wavelength ratios]

6 Conclusions

The study has investigated the second harmonic generation due to S_0 dominated, A_0 dominated, and S_0 and A_0 mixed incident Lamb wave interaction with the fatigue crack. In the experimental study, the results have shown that the S_0 dominated incident wave is more sensitive to the fatigue crack compared to the A_0 dominated, S_0 and A_0 mixed incident Lamb wave. In the numerical study, the piezoceramic actuator and sensor model have been implemented in the 3D FE simulations and there has been good agreement between the numerical and experimental results for the linear Lamb wave signal and the directivity pattern of the second harmonic generation. This has proved that the FE is not only capable of modeling the linear Lamb wave propagation,

but also the directivity pattern of the second harmonic generation due to the contact nonlinearity at the fatigue crack.

The results of the parametric study have shown that the magnitude of the second harmonic Lamb wave induced at the fatigue crack is dominant in the forward and backward scattering direction. In addition, the magnitude of the second harmonic Lamb wave in the forward scattering direction increases with the crack length to incident wave wavelength ratio at a higher rate compared to other directions. It is also found that S_0 Lamb wave has the dominant effect on second harmonic generation at the fatigue crack. Overall, this study has gained physical insights into the generation of the second harmonic due to the contact nonlinearity at a fatigue crack. The findings of this study help to further advance the use of the second harmonic Lamb wave for damage detection.

Acknowledgement

This work was supported by the Australian Research Council (ARC) under Grant Numbers DP160102233 and DE130100261. The supports are greatly appreciated.

References

[1] L.J. Rose, A baseline and vision of ultrasonic guided wave inspection potential, J. Press. Vess. Tech. 124 (2002) 273-282.

[2] V. Giurgiutiu, J. Bao, Embedded-ultrasonic structural radar for in situ structural health monitoring of thin-wall structures, Struct. Health Monitor. 3 (2004) 121-140.

[3] P. Aryan, A. Kotousov, C.T. Ng, B. Cazzolato, B, A baseline-free and non-contact method for detection and imaging of structural damage using 3D laser vibormetry. Struct. Cont. Health Monitor. 24 (2017) 1-13.

[4] K. Diamanti, C. Soutis, Structural health monitoring techniques for aircraft composite structures, Progress in Aerospace Sci. 46 (2010) 342-352.

[5] G. Giridhara, V.T. Rathod, S. Naik, D. Roy Mahapatra, S. Gopalakrishnan, Rapid localization of damage using a circular sensor array and Lamb wave based triangulation, Mech. Syst. Sig. Process. 24 (2010) 2929-2946.

[6] Y.K. An, H. Sohn, Integrated impedance and guided wave based damage detection, Mech. Syst. Sig. Process. 30 (2012) 157-167.

[7] C.T. Ng, On the selection of advanced signal processing techniques for guided wave damage identification using a statistical approach, Eng. Struct. 67 (2014) 50-60.

[8] T. Wandowski, P.H. Malinowski, W.M. Ostachowicz, Circular sensing networks for guided waves based structural health monitoring, Mech. Syst. Sig. Process. 66-67 (2016) 248-267.

[9] S. He, C.T. Ng, A probabilistic approach for quantitative identification of multiple delaminations in lamented composite beams using guided wave, Eng. Struct. 127 (2016) 602-614.

[10] S. He, C.T. Ng, Analysis of mode conversion and scattering of guided waves at cracks in isotropic beams using a time-domain spectral finite element method. Elec. J. Stuct. Eng. 14 (2015) 20-32.

[11] L. Moreau, A. Velichko, P.D. Wilcox, Accurate finite element modeling of guided wave scattering form irregular defects, NDT&E Inter. 45 (2012) 46-54.

[12] F. Casadei, J.J. Rimoli, M. Ruzzene, Multiscale finite element analysis of elastic wave scattering from localized defects, Finite Elements Analy Design 88 (2014) 1-15.

[13] C.T. Ng, On accuracy of analytical modeling of Lamb wave scattering at delaminations in multilayered isotropic plates, Inter. J. Struct. Stab. Dyn. 15 (2015) 1540010.

[14] C.T. Ng, A two-stage approach for quantitative damage imaging in metallic plates using Lamb waves, Earthquake & Struct. 8 (2015) 821-841.

[15] R. Carandente, A. Lovstad, P. Cawley, The influence of sharp edges in corrosion profiles on the reflection of guided waves, NDT&E Inter. 52 (2012) 57-68.

[16] R. Soleimanpour, C.T. Ng, Scattering of the fundamental anti-symmetric Lamb wave at through-thickness notches in isotropic plates. J. Civil Struct. Health Monitor. 6 (2016) 447-459.

[17] S. He, C.T. Ng, Guided wave-based identification of multiple cracks in beams using a Bayesian approach, Mech. Syst. Sig. Process. 84 Part A (2017) 324-345.

[18] X. Zhu, P. Rizzo, A. Marzani, J. Bruck, Ultrasonic guided waves for nondestructive evaluation/structural health monitoring of trusses. Meas. Sci. Technol. 21 (2010) 045701.

[19] P. Aryan, A. Kotousov, C.T. Ng, B. Cazzolato, A model-based method for damage detection with guided waves, Struct. Cont. Health Monitor. 24 (2017) 1-14.

[20] Y.K. An, H. Sohn, Instantaneous crack detection under varying temperature and static loading conditions, Struct. Health Monitor. 17 (2010) 730-741.

[21] A. Marzani, S. Salamone, Numerical prediction and experimental verification of temperature effect on plate waves generated and received by piezoceramic sensors, Mech. Syst. Sig. Process, 30 (2012) 204-217.

[22] P. Aryan, A. Kotousov, C.T. Ng, S. Wildy, Reconstruction of baseline time-trace under changing environmental and operational conditions, Smart Mater. Struct. 25 (2016) 035018.

[23] M. Mohabuth, A. Kotousov, C.T. Ng, Effect of uniaxial stress on the propagation of higher-order Lamb wave modes, Inter. J. Non-linear Mech. 86 (2016) 104-111.

[24] C. Bermes, J.Y. Kim, J. Qu, L.J. Jacobs, Nonlinear Lamb waves for the detection of material nonlinearity, Mech. Syst. Sig. Process. 22 (2008) 638-646.

[25] I. Solodov, J. Wacker, K. Pfleiderer, G. Busse, Nonlinear self-modulation and subharmonic acoustic spectroscopy for damage detection and location, Appl. Phys. Lett. 84 (2004) 5386-5388.

[26] F. Aymerich, W.J. Staszewski, Experimental study of impact-damage detection in composite laminates using a cross-modulation vibro-acoustic technique, Struct. Health Monitor. 9 (2010) 541-553.

[27] H.J. Lim, H. Sohn, fatigue crack detection using structural nonlinearity reflected on linear ultrasonic features, J. App. Phy. 118 (2015) 244902.

[28] K. Van Den Abeele, J. Carmeliet, J.A. TenCate, P.A. Jonson, Nonlinear elastic wave spectroscopy (NEWS) techniques to discern material damage, Part II: single-mode nonlinear resonance acoustic spectroscopy, Res. Nondestruct. Eval. 12 (2000) 31-42.

[29] J.H. Cantrell, W.T. Yost, Nonlinear ultrasonic characterization of fatigue microstructures, Int. J. Fatigue 23 (2001) S487-490.

[30] D.J. Barnard, G.E. Dace, O. Buck, Acoustic harmonic generation due to thermal embrittlement of Inconel 718, J. Nondestr Eval. 16 (1997) 67-75.

[31] S. Biwa, S. Hiraiwa, E. Matsumoto, Experimental and theoretical study of harmonic generation at contacting interface, Ultrasonics 44 (2006) e1319-e1322.

[32] K.H. Matlack, J.Y. Kim, L.J. Jacobs, J. Qu, Review of second harmonic generation measurement techniques for material state determination in metals, J. Nondestr Eval. 273 (2015) 1-23.

[33] K.Y. Jhang, Nonlinear ultrasonic techniques for non-destructive assessment of micro damage in material: A review, Inter. J. Precision Eng. Manu. 10 (2009) 123-135.

[34] C. Pruell, J.Y. Kim, J. Qu, L.J. Jacobs, A nonlinear-guided wave technique for evaluating plasticity-driven material damage in a metal plate, NDT&E Inter. 42 (2009) 199-203.

[35] Y. Shen, V. Giurgiutiu, Predictive modeling of nonlinear wave propagation of structural health monitoring with piezoelectric wafer active sensor, J. Intell. Mater. Syst. Struct. 25 (2014) 506-520.

[36] R. Soleimanpour, C.T. Ng, Locating delaminations in laminated composite beams suing nonlinear guided waves, Eng. Struct. 131 (2017) 207-219.

[37] W. Li, Y. Cho, J.D. Achenbach, Detection of thermal fatigue in composites by second harmonic Lamb waves, Smart Mater. Struct. 21 (2012) 085019.

[38] C. Zhou, M. Hong, Z. Su, Q. Wang, L. Cheng, Evaluation of fatigue cracks using nonlinearities of acousto-utlrasonic waves acquired by an active sensor network, Smart Mater. Struct. 22 (2013) 015018.

[39] V.K. Chillara, C.J. Lissenden, Review of nonlinear ultrasonic guided wave nondestructive evaluation: theory, numerics, and experiments, Optical Eng. 55 (2016) 011002.

[40] R. Soleimanpour, C.T. Ng, Higher harmonic generation of guided waves at delaminations in laminated composite beams. Struct. Health. Monitor. 2016 doi:10.1177/1475921716673021.

[41] N. P. Yelve, M. Mitra, P.M. Mujumdar, Detection of delamination in composite laminates using Lamb wave based nonlinear method. Comp. Struct. 159 (2017) 257-266.

[42] C. Nucera, F. Lanza di Scalea, Monitoring load levels in multi-wire strands by nonlinear ultrasonic waves, Struct. Health Monitor. 10 (2011) 617-629.

[43] B. Lee, W. Staszewski, Modelling of Lamb waves for damage detection in metallic structures: Part I. Wave propagation, Smart Mater. Struct. 12(5) (2003) 804-814.

[44] S. Gopalakrishnan, A. Chakraborty, D. Mahapatra, Spectral finite element method, wave propagation, diagnostics and control in anisotropic and inhomogeneous Structures, Springer Science & Business media, 2007.

[45] W. Ostachowicz, P. Kudela, M. Krawczuk, A. Zak, Guided waves in structures for SHM: the time-domain spectral element method, John Wiley & Sons, 2011.

[46] P. Kudela, W. Ostachowicz, 3D time-domain spectral elements for stress waves modelling, J. Phys.: Conference series 181(1) (2009) doi:10.1088/1742-6596/181/1/012091

[47] X. Lin and F.G. Yuan, Diagnostic Lamb waves in an integrated piezoelectric sensor/actuator plate: analytical and experimental studies, Smart Mater. Struct. 10 (2001) 907-913.

[48] Z. Su, L. Ye, Lamb Wave Propagation-based Damage Identification for Quasi-isotropic CF/EP Composite Laminates Using Artificial Neural Algorithm: Part I - Methodology and Database Development, J. Intell. Mater. Syst. Struct. 16 (2005) 97-111.

[49] P.J. Blau, Friction Science and Technology, CRC Press, 2009.

[50] H. Sohn, S.J. Lee, Lamb wave tuning curve calibration for surface-bonded piezoelectric transducers, J Smart Mater. Struc. 19 (2010) 015007.

[51] N. Yelve, M. Mitra, P. Mujumdar, Spectral damage index for estimation of breathing crack depth in an aluminum plate using nonlinear Lamb wave, Struct. Control Health Monit. 21(5) (2014) 833-846.

[52] T.H. Lee, K.Y. Jhang, Experimental investigation of nonlinear acoustic effect at crack, NDT&E Inter. 42 (2009) 757-764.

[53] J. Codrington, A. Kotousov, The distributed dislocation technique for calculating plasticity-induced crack closure in plates of finite thickness, Inter J. Fracture. 144 (2007) 285-295.

Figure List

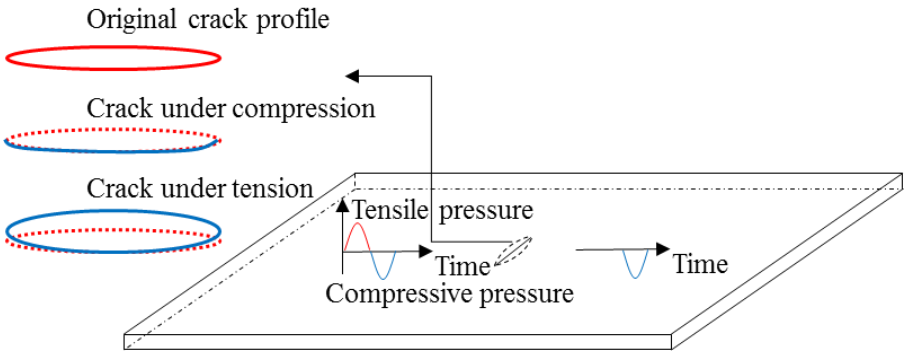

Figure 1: Concept of contact nonlinearity at a fatigue crack

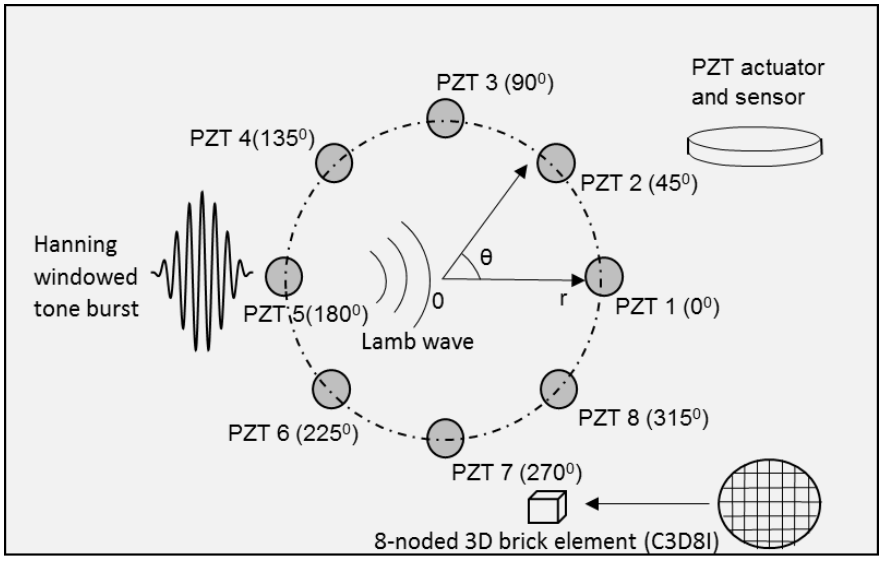

Figure 2: Schematic diagram of FE simulations and experiments

a) 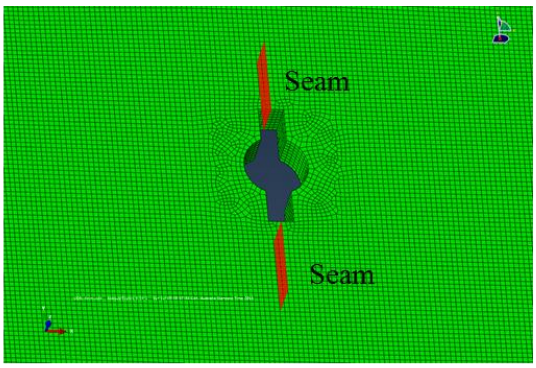

b) 

Figure 3: FE model of the fatigue crack for simulating the a) experimental condition, and b) numerical parametric study

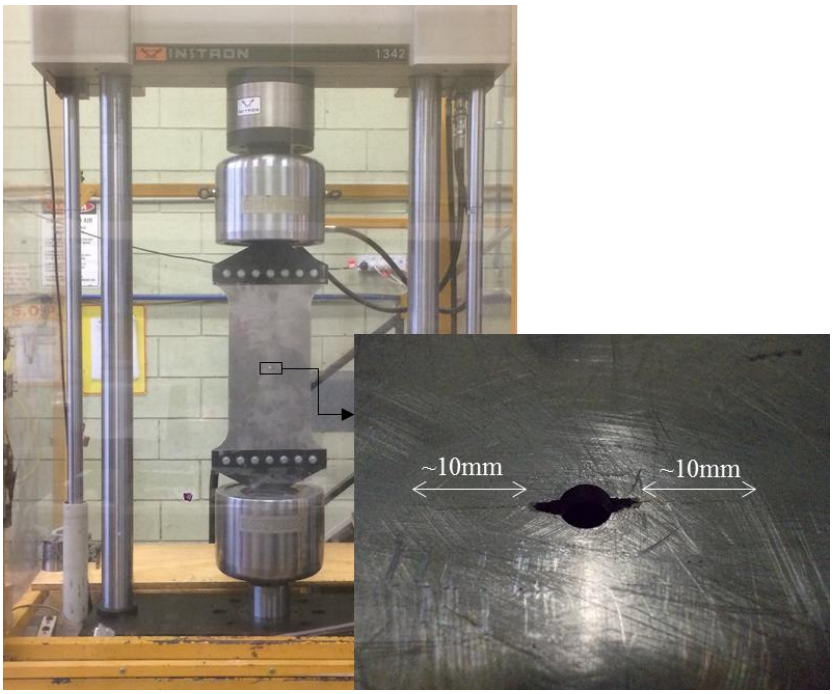

Figure 4: Fatigue testing using INSTRON and the fatigue crack generated at the end of the starter notches

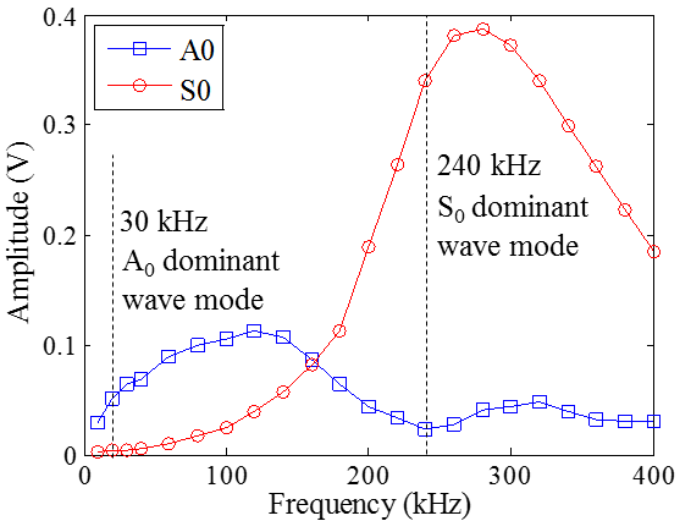

Figure 5: Lamb wave mode-turning curve for 3mm thick 5005-H34 aluminum plate excited by a 10mm diameter and 5mm thick piezoceramic disc

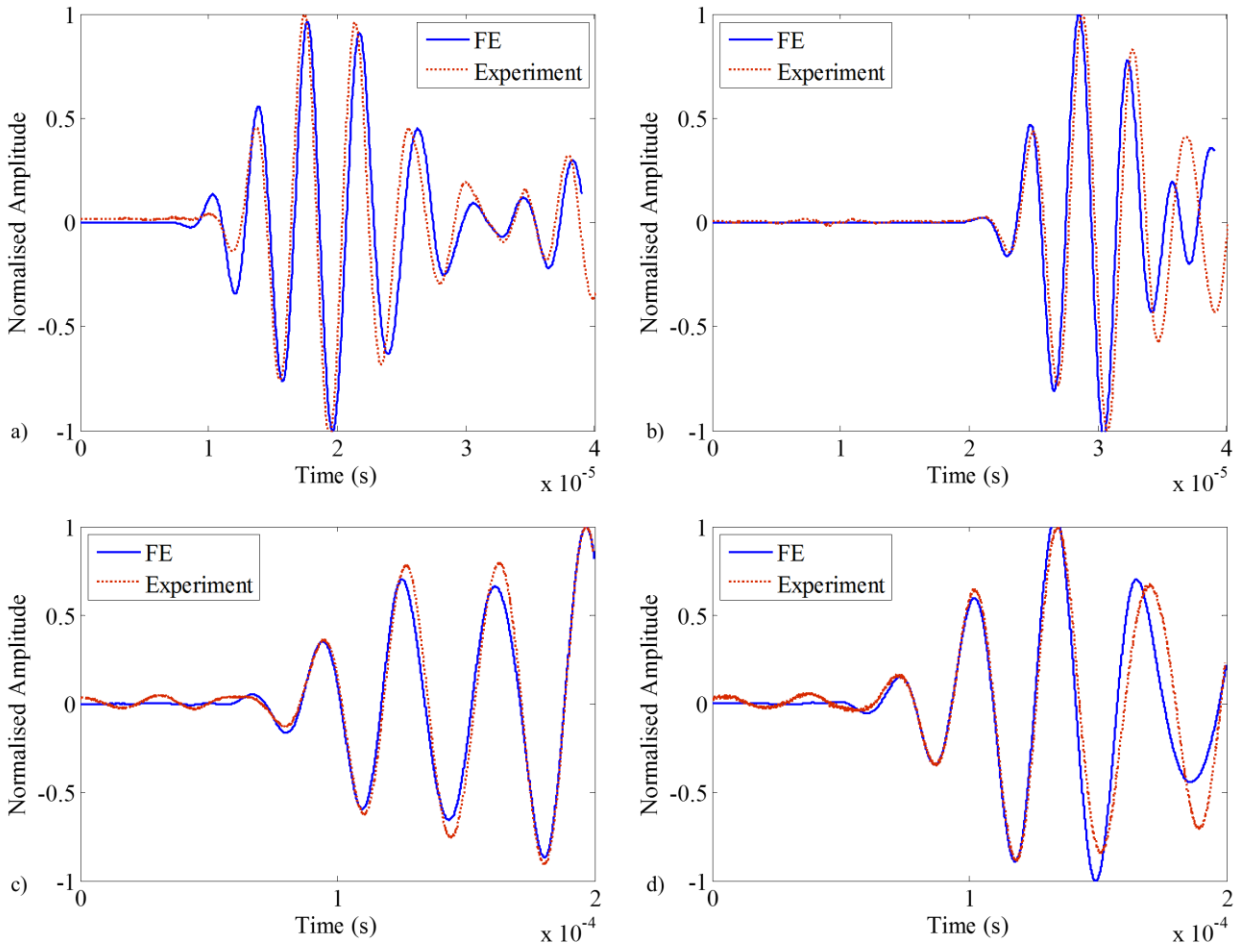

Figure 6: Numerical simulated and experimental measured Lamb wave signal, a): 30 kHz wave at PZT2, b): 30kHz wave at PZT4, c): 240kHz wave at PZT2, and d): 240kHz wave at PZT4

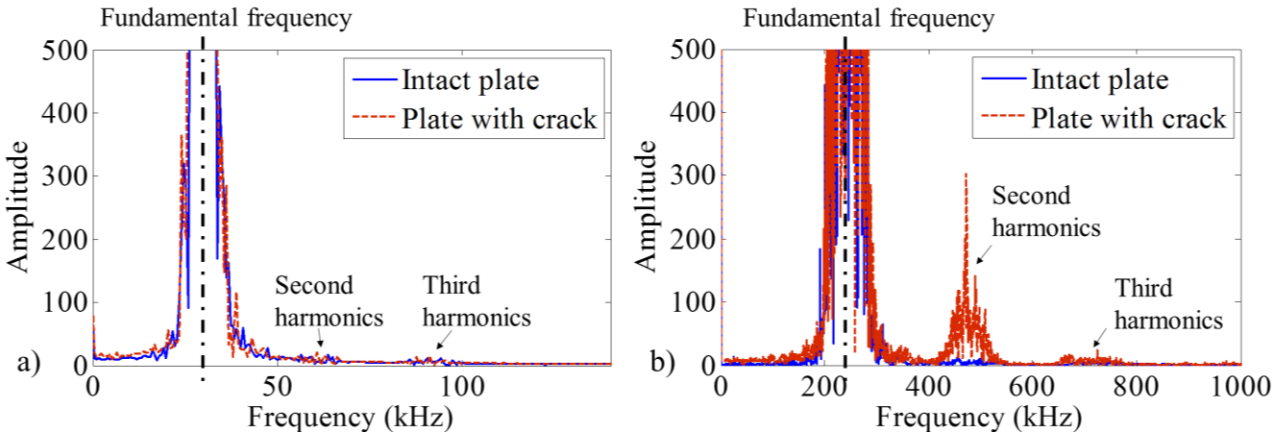

Figure 7: Spectra of the signals measured by PZT6 of the intact plate and the plate with the fatigue crack for the incident a) A_0 (30kHz) and b) S_0 Lamb wave (240kHz)

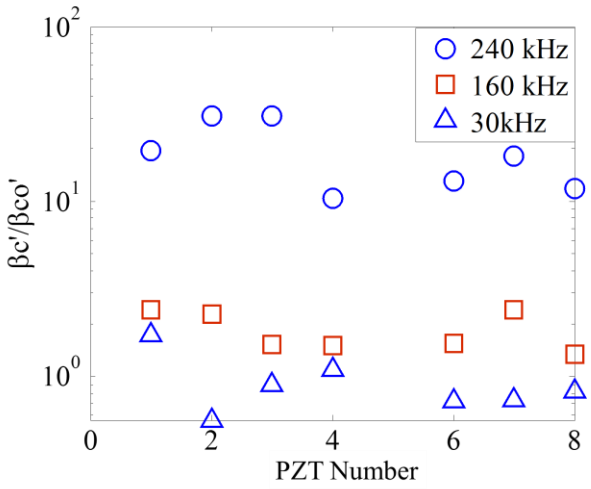

Figure 8: Experimentally obtained normalized relative nonlinear parameter at all transducers on the damaged plate using 240kHz (S_0) and 160kHz (S_0 and A_0) and 30kHz (A_0) incident Lamb wave

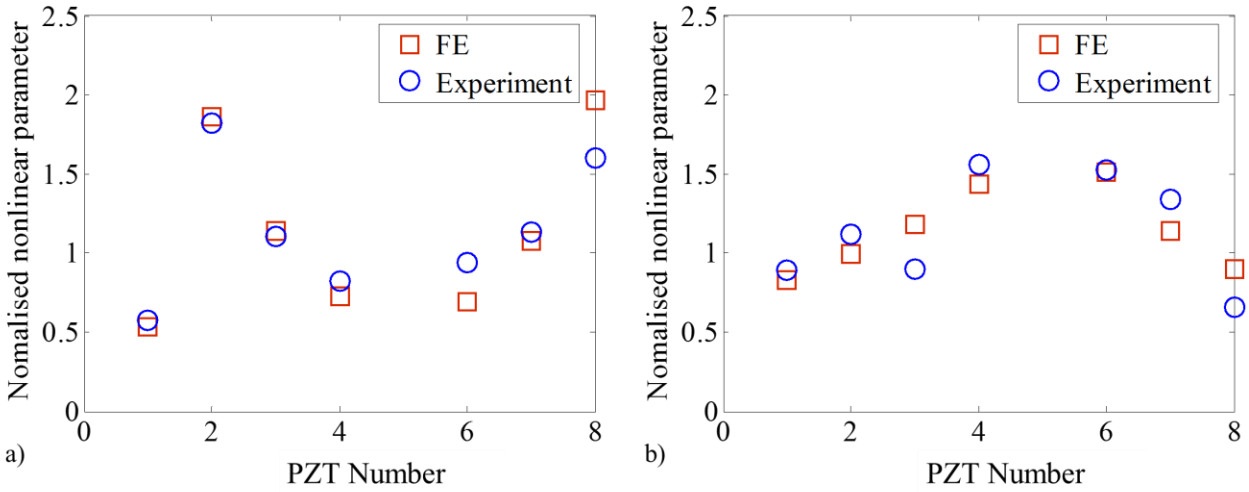

Figure 9: FE simulated and experimentally measured normalized relative nonlinear parameter at a) 240 kHz (S_0 Lamb wave); and b) 160kHz (S_0 and A_0 mixed Lamb wave)

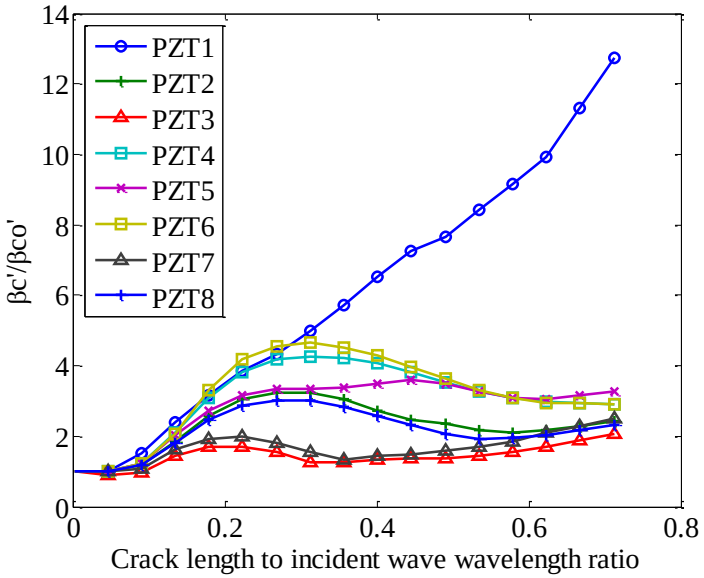

Figure 10: Normalized relative nonlinear parameter as a function of fatigue crack length to incident wave wavelength ratio

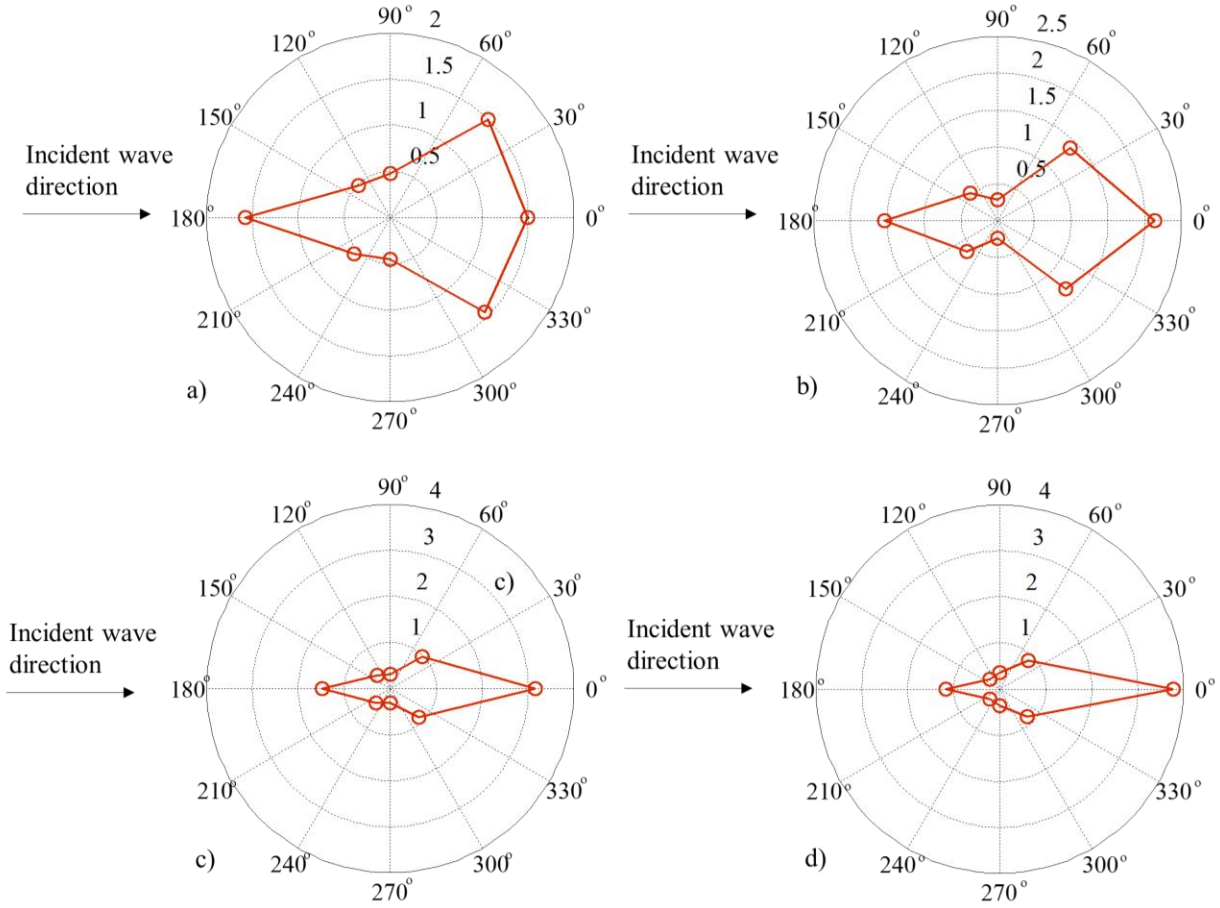

Figure 11: Directivity pattern of normalized relative nonlinear parameters for a) 4 mm; b) 8 mm; c) 12 mm; and d) 16 mm long fatigue crack

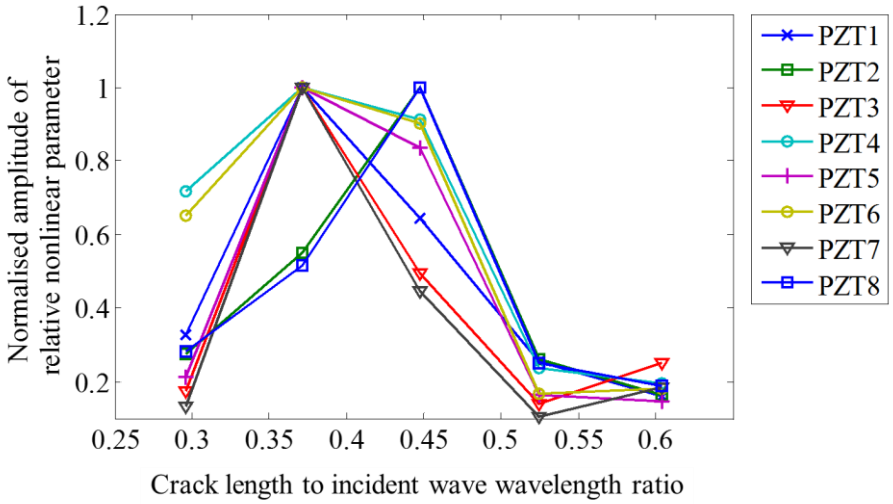

Figure 12: Variation of normalized relative nonlinear parameter against the crack length to incident wave wavelength ratio.

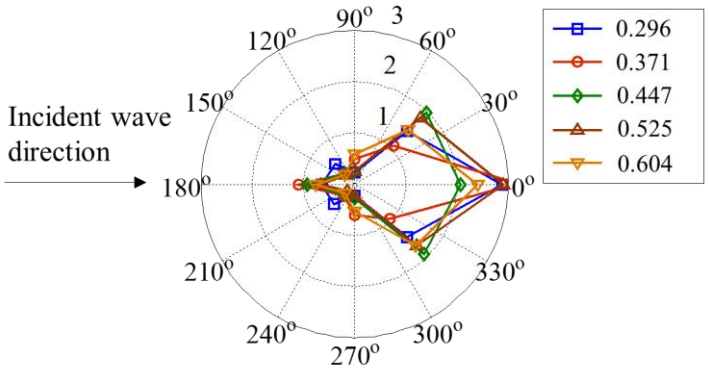

Figure 13: Directivity patterns of normalized relative nonlinear parameters at different crack length to incident wave wavelength ratios.

Table List

Table 1: Material properties of the piezoceramic discs

Young's modulus	Poisson's ratio	Density	Relative dielectric constant K_3	Piezoelectric charge constant d_{31}	Dielectric permeability p_0
59GPa	0.389	7700kg/m^3	1800	170×10^{-12}m/V	8.85×10^{-12}F/m